This article is made available via the ACS COVID-19 subset for unrestricted RESEARCH re-use and analyses in any form or by any means with acknowledgement of the original source. These permissions are granted for the duration of the World Health Organization (WHO) declaration of COVID-19 as a global pandemic.

ACS APPLIED NANO MATERIALS

www.acsanm.org Article

DNA-Functionalized $Ti_3C_2T_x$ MXenes for Selective and Rapid Detection of SARS-CoV-2 Nucleocapsid Gene

Winston Yenyu Chen,[⊥] Hang Lin,[⊥] Amit Kumar Barui, Ana Maria Ulloa Gomez, Michael K. Wendt, and Lia A. Stanciu*

Cite This: *ACS Appl. Nano Mater.* 2022, 5, 1902−1910 Read Online

ACCESS | Metrics & More | Article Recommendations | Supporting Information

ABSTRACT: Coronavirus disease 2019 (COVID-19) is an emerging human infectious disease caused by severe acute respiratory syndrome 2 (SARS-CoV-2, initially called novel coronavirus 2019-nCoV) virus. Thus, an accurate and specific diagnosis of COVID-19 is urgently needed for effective point-of-care detection and disease management. The reported promise of two-dimensional (2D) transition-metal carbides ($Ti_3C_2T_x$ MXene) for biosensing owing to a very high surface area, high electrical conductivity, and hydrophilicity informed their selection for inclusion in functional electrodes for SARS-CoV-2 detection. Here, we demonstrate a new and facile functionalization strategy for $Ti_3C_2T_x$ with probe DNA molecules through noncovalent adsorption, which eliminates expensive labeling steps and achieves sequence-specific recognition. The 2D $Ti_3C_2T_x$ functionalized with complementary DNA probes shows a sensitive and selective detection of nucleocapsid (N) gene from SARS-CoV-2 through nucleic acid hybridization and chemoresistive transduction. The fabricated sensors are able to detect the SARS-CoV-2 N gene with sensitive and rapid response, a detection limit below 10^5 copies/mL in saliva, and high specificity when tested against SARS-CoV-1 and MERS. We hypothesize that the MXenes' interlayer spacing can serve as molecular sieving channels for hosting organic molecules and ions, which is a key advantage to their use in biomolecular sensing.

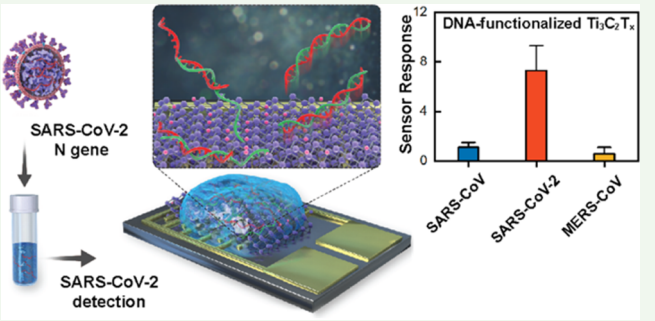

KEYWORDS: *SARS-CoV-2, diagnostic, COVID-19, biosensor, $Ti_3C_2T_x$, DNA hybridization, pandemic*

Downloaded via PURDUE UNIV on November 9, 2023 at 17:47:06 (UTC).
See https://pubs.acs.org/sharingguidelines for options on how to legitimately share published articles.

INTRODUCTION

Coronavirus disease 2019 (COVID-19) pandemic was first detected in December 2019 in Wuhan, China and has caused a global outbreak and a serious public health concern. The novel coronavirus was named severe acute respiratory syndrome 2 (SARS-CoV-2, initially named 2019-nCoV), the pathogen causing COVID-19, which causes respiratory and intestinal illness in both humans and animals. As of mid-October 2021, the rapid spread of SARS-CoV-2 has impacted more than 200 countries, infecting more than 240 million people with over 4 million confirmed deaths.[1] COVID-19/SARS-CoV-2 is still devastating people and countries around the world and seems to be difficult to tackle at this moment. There have been other recurrent outbreaks from emerging coronaviruses, such as severe acute respiratory syndrome (SARS-CoV-1) in 2003 and Middle East respiratory syndrome (MERS-CoV) in 2012. Thus, there is a critical need for the development of a rapid, inexpensive, and reliable identification method toward novel viruses that can greatly facilitate public health response to emerging viral threats.

Real-time reverse transcription-polymerase chain reaction (real-time RT-PCR) is one of the most widely used laboratory methods for the detection of SARS-CoV-2 using samples from respiratory secretions.[2] The targets for RT-PCR molecular assays developed by various countries are genetically similar. The national RT-PCR protocols among various countries typically target the nucleocapsid (N) gene of SARS-CoV-2 due to its highly conserved nature and few nucleotide changes over time.[3] RT-PCR is highly sensitive and specific for detecting viral RNA by amplification of specific sequence regions.[4] However, molecular diagnosis using RT-PCR presents some drawbacks, including expensive fluorescent tags, long processing time, tedious sample preparation, need for laboratory facilities, and manpower issues, limiting testing capacity during large-scale outbreaks. Thus, there is still an urgent need to develop rapid and accurate diagnostic technologies for the detection of SARS-CoV-2.

Biosensors are promising candidates for providing an alternative and reliable solution to clinical diagnosis, real-

Received: October 20, 2021
Accepted: December 16, 2021
Published: December 30, 2021

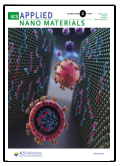

ACS Publications © 2021 American Chemical Society

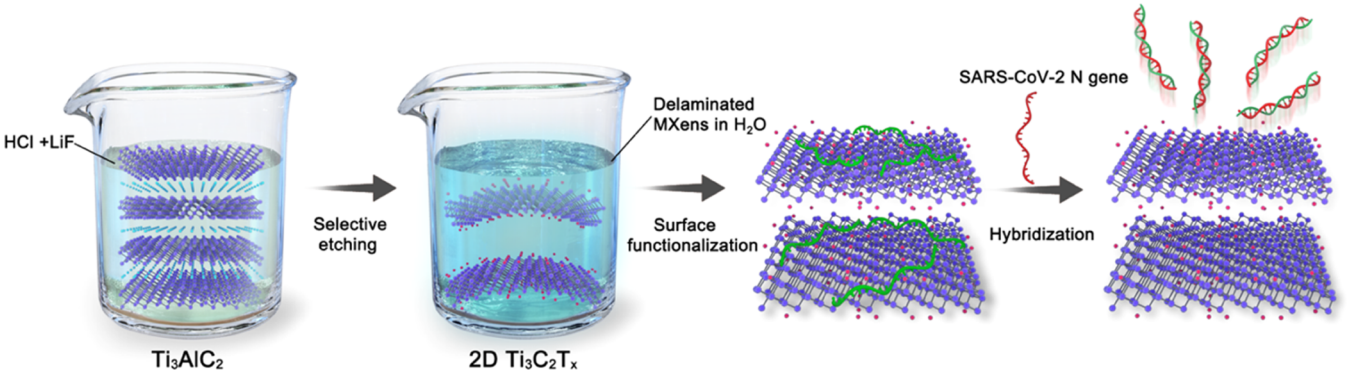

Figure 1. Schematic illustration of the process for etching and delamination of $Ti_3C_2T_x$ MXenes and surface functionalization of $Ti_3C_2T_x$ with ssDNA probes, forming ssDNA/$Ti_3C_2T_x$ biosensors for the selective detection of SARS-CoV-2 nucleocapsid (N) gene.

time detection, and on-site monitoring.[5] Compared with the RT-PCR technique, electronic-based biosensors present the advantages of low cost, high speed, small size, and label-free detection, leading to the possibility of widespread biomedical applications. A recent report used thiolated-DNA-functionalized gold nanoparticles to detect SARS-CoV-2 sequences based on the laser-induced plasmonic photothermal reaction.[6] The field-effect transistor based on graphene conjugated with SARS-CoV-2 spike antibody was used to detect the SARS-CoV-2 spike protein via the antibody−antigen reaction.[7] Carbon nanotubes were functionalized with a host protein for the detection of SARS-CoV-2 spike protein based on an optical sensing approach.[8] In another report, SARS-CoV-2 viral particles were detected via electrochemical methods through the same antibody binding of spike protein.[9]

Notably, detection of pathogens, including viruses, by recording changes in the surface electrical properties of electrodes upon DNA hybridization, interfacing with two-dimensional (2D) materials has recently received extensive attention.[10] This sensing modality offers a specificity that is as high as that of RT-PCR, but without the use of fluorescent probes or laboratory-scale signal-transducing instruments, which significantly lower the detection cost, along with the advantage of higher-field deployability and faster potential turnaround to results.[11] Owing to their large surface area and unique electrical/optical properties, 2D materials, such as graphene, molybdenum disulfide (MoS_2), and tungsten disulfide (WS_2),[12,13] offer highly sensitive sensing channels for the development of novel biosensors. Although lateral flow assays (LFA) have been demonstrated for the detection of pathogens, they suffer from a poor analytical sensitivity in comparison to electronic-based biosensors.[4]

MXenes, a new family of multifunctional 2D transition-metal carbides/nitrides with various intriguing properties, have been developed by Gogotsi and co-workers.[14−16] They are typically prepared by selectively etching away intermediate A layers from MAX ($M_{n+1}AX_n$) phases, which have a general formula of $M_{n+1}X_nT_x$, where M stands for an early transition metal, A is a A group element, X is carbon and/or nitrogen, and T_x represents surface functional groups such as −O, −OH, and/or −F. MXenes have a unique combination of properties, including metallic conductivity, surface hydrophilicity, large chemically active surface, high specific surface, and good mechanical properties and thus are promising for numerous applications including energy storage,[17] electromagnetic shielding,[18] water purification,[19] catalysis,[20] and chemical sensors.[21] However, MXenes have rarely been employed in biosensing applications. It has been recently reported that MXenes are also biocompatible and hold a great potential in biomedical applications,[22,23] such as drug delivery and biomolecule adsorption using their abundant surface anchoring sites.[24−26]

Another 2-D material, graphene, by comparison, has been extensively used in biosensors. Such graphene-based biosensors typically show low sensitivity and small changes in electrical conductance owing to the zero-band-gap electronic structure of graphene.[7,11,27] Although yet another 2D material class, transition-metal dichalcogenides (TMDCs) have a larger band gap and exhibit a higher sensitivity for biosensing, the high electrical noise level limits their practical use, even when lab-based performance is adequate.[12,28] In contrast, MXene-based biosensors have advantages of ultrahigh electrical conductivity, hydrophilic surface, offering not only a high signal-to-noise ratio for chemiresistive biosensors but also the ability to precisely tailor their properties for biomolecule sensing through surface modification. Thus, the MXenes are interesting candidates to investigate the development of high-performance biosensors. The functionalization strategy for 2D materials (e.g., graphene, MoS_2, and $Ti_3C_2T_x$) is mainly based on noncovalent interactions and simple adsorption of biomolecules,[13,29,30] including $\pi-\pi$ stacking, hydrogen bonding, and van der Waals interactions.[31]

Herein, we report on the development of single-stranded DNA functionalization of $Ti_3C_2T_x$ MXene (ssDNA/$Ti_3C_2T_x$) and its novel use in a chemoresistive biosensing platform for the highly sensitive and fast detection of SARS-CoV-2 N gene. The 2D $Ti_3C_2T_x$ surfaces were used for the first time in such a biosensing platform and were functionalized by SARS-CoV-2 N gene-specific nucleic acid probes through noncovalent adsorption, which enables sequence-specific detection via hybridization with target SARS-CoV-2 genes. Targeting the N gene rather than the more often targeted protein S is another novel feature of this work along with the unique and simple, compared to other reports, chemoresistive mechanism.[7,32] The hybridization of SARS-CoV-2 N gene with complementary DNA probes leads to the detachment of hybridized double-stranded molecules from the $Ti_3C_2T_x$ surface, resulting in an increase in the conductivity of the $Ti_3C_2T_x$ channel. Importantly, ssDNA/$Ti_3C_2T_x$ biosensors detect SARS-CoV-2 N gene with a very low limit of detections of below 10^5 copies/mL in saliva and a fast response. The capability of ssDNA/$Ti_3C_2T_x$ biosensors developed here to distinguish the SARS-CoV-2 N gene from those of SARS-CoV-1 and MERS-CoV is presented, thus providing the feasibility of

https://doi.org/10.1021/acsanm.1c03520
ACS Appl. Nano Mater. 2022, 5, 1902−1910

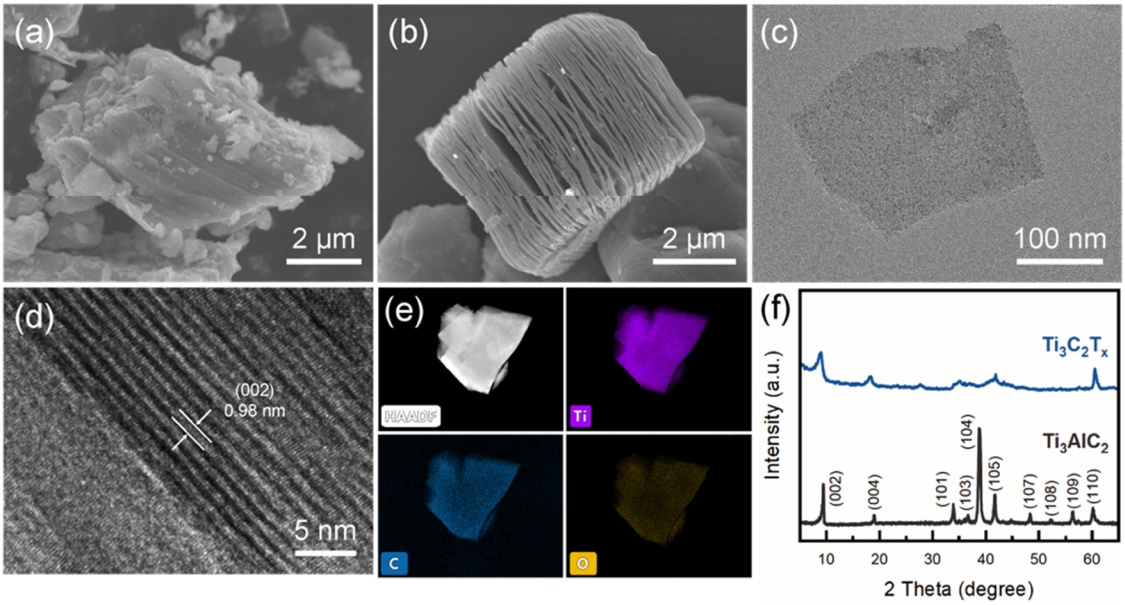

Figure 2. SEM images of (a) Ti_3AlC_2 powder and (b) accordion-like $Ti_3C_2T_x$ MXene. (c) TEM image of an exfoliated $Ti_3C_2T_x$ nanosheet. (d) High-resolution TEM image of $Ti_3C_2T_x$ nanosheets with a lattice distance of 0.98 nm. (e) HAADF-STEM image and corresponding elemental mapping of Ti, C, and O for $Ti_3C_2T_x$. (f) XRD patterns of Ti_3AlC_2 and $Ti_3C_2T_x$ powders.

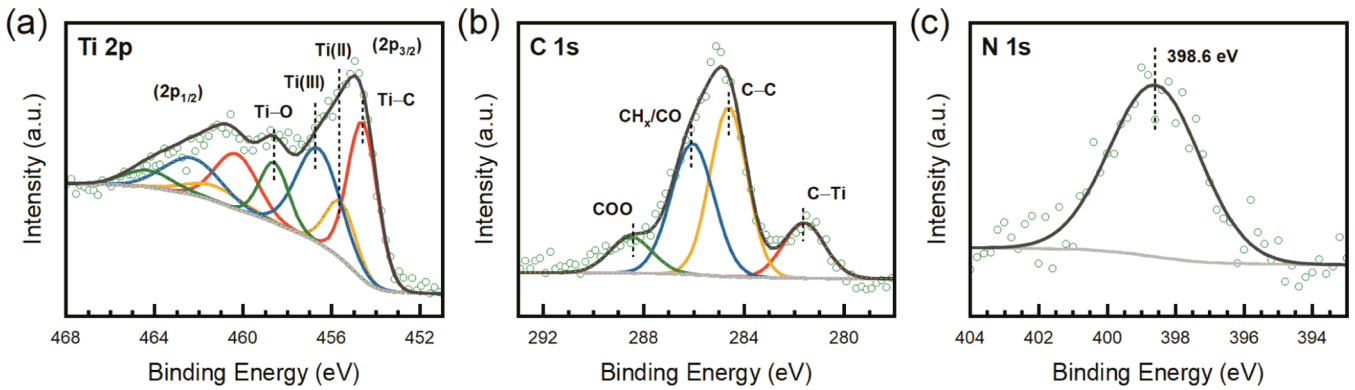

Figure 3. Chemical composition and bonding configurations of as-prepared DNA-functionalized $Ti_3C_2T_x$ MXene. High-resolution XPS spectra of (a) Ti 2p, (b) C 1s, and (c) N 1s from ssDNA/$Ti_3C_2T_x$ films.

developing a new and highly specific and sensitive MXene-based testing technology for the rapid diagnosis of COVID-19.

RESULTS AND DISCUSSION

Figure 1 shows the preparation of ssDNA/$Ti_3C_2T_x$ biosensors for SARS-CoV-2 detection. First, the $Ti_3C_2T_x$ MXene was synthesized by the selective etching of Al layers from their Ti_3AlC_2 MAX phase in a HCl−LiF premixed solution and further delaminated in water by ultrasonication. The $Ti_3C_2T_x$ dispersions were then spray-coated onto gold interdigitated electrodes. The detailed procedure for device fabrication is given in the Experimental Section. For the selective detection of SARS-CoV-2 N gene, $Ti_3C_2T_x$ films were functionalized with DNA probes through noncovalent binding based on weak interactions involving the phosphate backbone and/or nucleobases.[30,33] The detection mechanism of SARS-CoV-2 N gene is based on sequence-specific hybridization. Specifically, when the ssDNA probe hybridizes with the target SARS-CoV-2 N gene (complementary sequences), the interaction between the formed double-strained DNA and layered $Ti_3C_2T_x$ is weakened, resulting in desorption of hybridized compounds off the MXene surface and thus increasing channel conductance. Moreover, only the specific bases of DNA can hybridize with their complementary sequences, which enhances the selectivity of the sensing platform.[13]

Figure 2a,b shows the scanning electron microscopy (SEM) images of Ti_3AlC_2 and as-etched $Ti_3C_2T_x$, respectively, indicating a successful transition from a bulk Ti_3AlC_2 to an accordion-like $Ti_3C_2T_x$ MXene with interlayer spacing that can serve as molecular sieving channels for hosting organic molecules and ions.[15] The increased interlayer spacing of $Ti_3C_2T_x$ MXene is induced by the selective etching, which in turn facilitates molecular transport and creates extra active sites for the electrochemical reaction. Previous studies have proposed a similar intercalation effect for different metal cations, organic molecules, and polymers, resulting in improved electrochemical performance of MXenes.[34−37] The transmission electron microscopy (TEM) imaging of delaminated $Ti_3C_2T_x$ nanosheets reveals quite thin, electron-transparent flakes with a typical size of about 200 nm (Figure 2c). The high-resolution TEM image in Figure 2d reveals a high crystallinity of $Ti_3C_2T_x$ nanosheets, with a lattice distance of

https://doi.org/10.1021/acsanm.1c03520
ACS Appl. Nano Mater. 2022, 5, 1902−1910

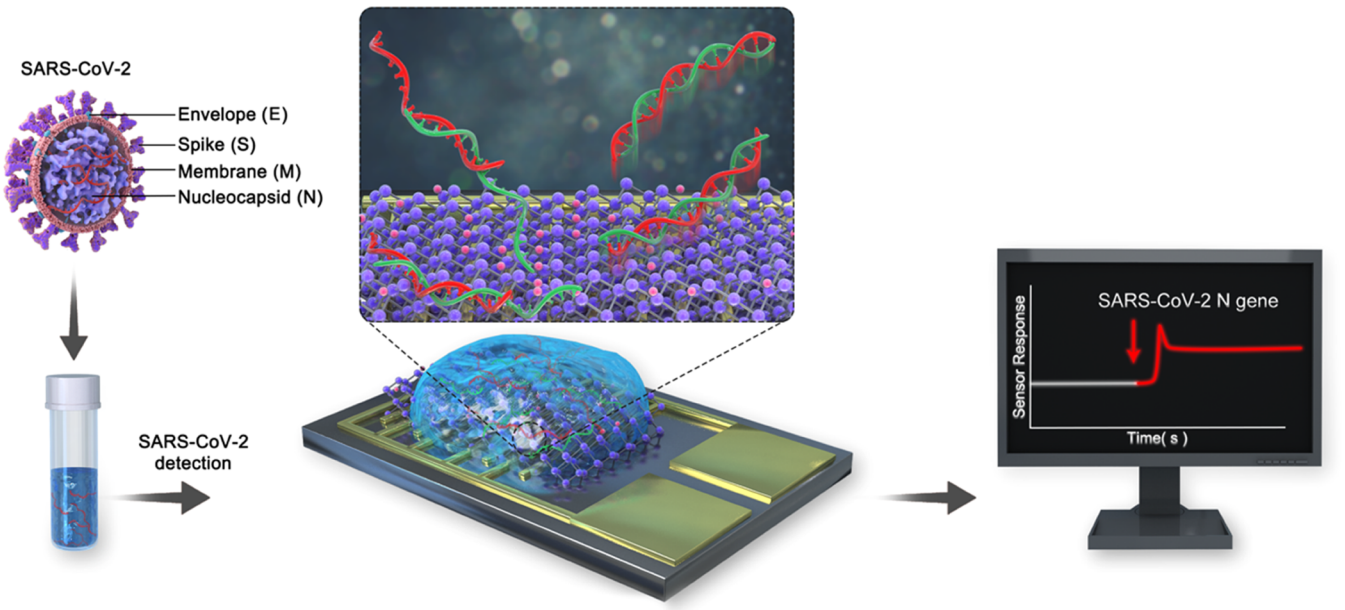

Figure 4. Schematics illustrating the operation of ssDNA/$Ti_3C_2T_x$ sensors for the detection of SARS-CoV-2 nucleocapsid (N) gene.

0.98 nm for the (002) plane of $Ti_3C_2T_x$, consistent with X-ray diffraction (XRD) analysis presented later. Moreover, the high-angle annular dark-field scanning transmission electron microscopy (HAADF-STEM) imaging, along with the associated energy-dispersive X-ray elemental mapping, presented in Figure 2e, shows a uniform distribution of Ti, C, and O elements in $Ti_3C_2T_x$ nanoflakes. The XRD patterns of Ti_3AlC_2 and as-etched $Ti_3C_2T_x$ are displayed in Figure 2f, further confirming the formation of $Ti_3C_2T_x$ MXene. After the selective etching of Ti_3AlC_2, an intense peak at 39.1°, corresponding to the (104) plane of Ti_3AlC_2, is greatly weakened, accompanied by a downshift of the (002) peak from 9.5 to 8.9°, indicating the removal of Al layers and a successful formation of the $Ti_3C_2T_x$ MXene.[38]

X-ray photoelectron spectroscopy (XPS) was used to investigate the element composition and bonding configuration of ssDNA-functionalized $Ti_3C_2T_x$ (see Figure 3, as well as Figure S1, Supporting Information). The survey spectra and atomic concentrations (Table S1, Supporting Information) of elements for both samples indicate that ssDNA functionalized has increased nitrogen concentration, which is a key element in nucleic acids' sequence. The high-resolution spectra of Ti 2p, C 1s, and N 1s (Figure 3), taken from ssDNA/$Ti_3C_2T_x$ films, also suggest the presence of DNA probes on $Ti_3C_2T_x$ MXene after surface functionalization. The high-resolution Ti 2p spectrum (Figure 3a) was fitted with four doublets (Ti $2p_{3/2}$ and Ti $2p_{1/2}$) with an area ratio of 2:1 and a doublet separation of 5.7 eV, characteristics of $Ti_3C_2T_x$.[39] The Ti 2p spectrum was deconvoluted into four peaks centered at 454.6, 455.6, 456.6, and 458.6 eV, corresponding to Ti−C, Ti^{2+}, Ti^{3+}, and Ti−O, respectively.[40] The C 1s spectrum in Figure 3b is fitted with four peaks centered at 281.6, 284.6, 286.1, and 288.5 eV, corresponding to C−Ti, C−C, CH_x/CO, and COO, respectively.[41] The N 1s peak is a reliable indication that DNA is adsorbed on the surface of $Ti_3C_2T_x$, as nitrogen is exclusively found in the nitrogen-containing base pairs of DNA.[42] The N 1s spectrum in Figure 3c can be identified with the binding energy value of 398.6 eV, demonstrating the successful adsorption of DNA onto the $Ti_3C_2T_x$ MXene surface.

Figures 4 and S2 in the Supporting Information show the detection mechanism of SARS-CoV-2 N gene using a $Ti_3C_2T_x$-based biosensing device functionalized with probe DNAs. When complementary SARS-CoV-2 N genes are introduced, the desorption of ssDNA probes out of the MXene surface induced by the hybridization process results in an increase in the conductance of the sensing channel. Due to the sequence-recognition property, noncomplementary genes will not be hybridized with ssDNA probes on the $Ti_3C_2T_x$ surface, which means that the sensing platform has sequence specificity. SARS-CoV-2 genomes encode four structural proteins, including spike (S), envelope (E), membrane (M), and nucleocapsid (N).[43] Among them, a virus surface S protein mediates SARS-CoV-2 entry into human cells, and thus it is considered as a major target for both vaccine design and rapid diagnosis.[44] However, the SARS-CoV-2 S gene shares 76% similarity of amino acid sequence to the SARS-CoV S gene, and nonsynonymous mutations develop in the S protein when the SARS-CoV-2 pandemic progress.[45−47] By contrast, SARS-CoV-2 N gene is genetically stable and allows for few gene mutations over time.[48] Owing to the sequence specificity of the sensing platform, it can be easily modified to address present and future emerging mutations in the virus' N gene, which can be targeted by designing new probe sequences. The N protein of many coronaviruses is also highly immunogenic and expressed abundantly during infection.[49] Thus, the N gene of SARS-CoV-2 should be a promising target candidate for rapid diagnosis of SARS-CoV-2.

US Centers for Disease Control and Prevention (CDC) published two specific sequences of probes, 2019-nCoV_N-F and 2019-nCoV_N-R, for the purposes of identifying SARS-CoV-2 N gene. We integrated these recognition probes with 2D MXenes for the development of COVID-19 sensors. To validate the presence of the ssDNA probes on the $Ti_3C_2T_x$ surface, the current−voltage (IV) curves of the fabricated $Ti_3C_2T_x$ before and after probe DNA functionalization were recorded. As shown in Figure 5a, the ssDNA functionalization

https://doi.org/10.1021/acsanm.1c03520
ACS Appl. Nano Mater. 2022, 5, 1902−1910

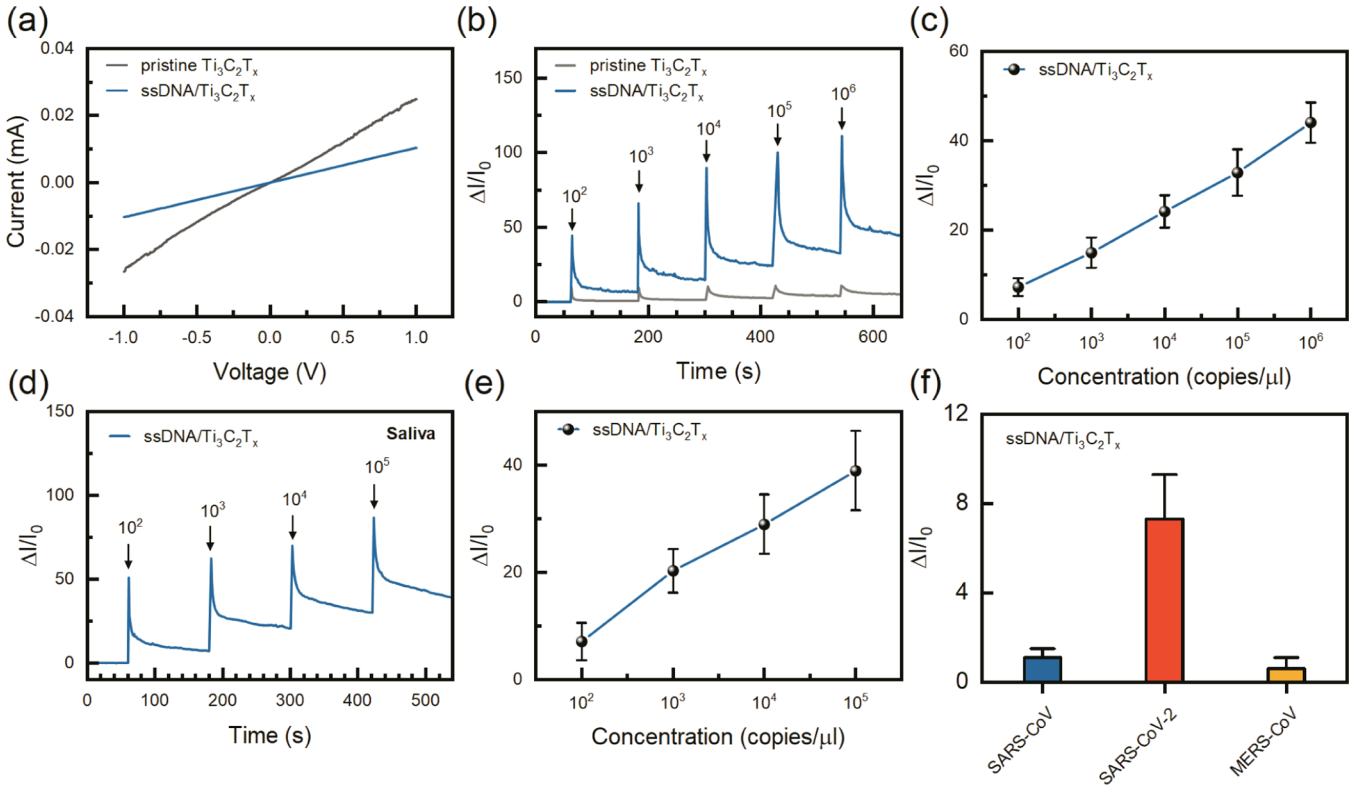

Figure 5. Detection of SARS-CoV-2 N gene using ssDNA/$Ti_3C_2T_x$ sensors. (a) Current−voltage (IV) curves of pristine $Ti_3C_2T_x$ and ssDNA-functionalized $Ti_3C_2T_x$ devices. (b) Real-time responses of $Ti_3C_2T_x$ and ssDNA/$Ti_3C_2T_x$ sensors toward different concentrations of SARS-CoV-2 N gene in buffer. (c) Response as a function of SARS-CoV-2 N gene concentrations for ssDNA/$Ti_3C_2T_x$ sensors ($\pm 1\sigma$; $N = 3$). (d) Real-time response of ssDNA/$Ti_3C_2T_x$ sensors toward different concentrations of SARS-CoV-2 N gene in artificial saliva and (e) corresponding response versus concentration plot for ssDNA/$Ti_3C_2T_x$ sensors. (f) Selectivity test of ssDNA/$Ti_3C_2T_x$ sensors toward different N gene from SARS-CoV-1, target SARS-CoV-2, and MERS-CoV, showing the selective detection of ssDNA/$Ti_3C_2T_x$ with SARS-CoV-2 N gene.

results in an increase in electrical resistance of the hosting $Ti_3C_2T_x$, indicating the successful introduction of ssDNA probes. With the loading of DNA probes, the electrical resistance of the sensors increases because of the metallic property of $Ti_3C_2T_x$ MXene.[28] To evaluate the performance of ssDNA/$Ti_3C_2T_x$ sensors for the detection of SARS-CoV-2 N gene, we performed the real-time measurements of ssDNA/$Ti_3C_2T_x$ sensors in a buffer solution with target SARS-CoV-2 N gene, using pristine $Ti_3C_2T_x$ sensors as a control (Figure 5b).

ssDNA/$Ti_3C_2T_x$ sensors produce a rapid spike in relative conductance ($-\Delta I/I_0$) upon adsorption of target DNA (SARS-CoV-2 N gene) before settling to steady-state values. The spike in $\Delta I/I_0$ indicates a transient perturbation in electronic states at the sensor surface caused by structural reorganization upon DNA hybridization. These findings indicate that only ssDNA-functionalized $Ti_3C_2T_x$ is sensitive to SARS-CoV-2 N gene over the concentration range from 10^5 to 10^9 copies/mL. The responses of ssDNA/$Ti_3C_2T_x$ sensors to concentration variations of SARS-CoV-2 N gene are displayed in Figure 5c, showing a nearly linear response to SARS-CoV-2 N gene over a wide range of concentrations, indicating a lower limit of detection and good reproducibility of sensing response. Notably, ssDNA-functionalized $Ti_3C_2T_x$ not only exhibits a high sensitivity to the target SARS-CoV-2 N gene but also provides an excellent detection limit, which further highlights the advantages of using ssDNA/$Ti_3C_2T_x$ chemiresistive sensors for SARS-CoV-2 viral nucleic acid quantitative detection. It is important to note that this detection limit is equal to the one offered by conventional laboratory-based RT-PCR detection.[50]

Moreover, diagnosis of COVID-19 using a saliva sample eliminates the need for nasopharyngeal swabs, which are invasive and prone to a shortage. The viral load of virus stays a longer period in saliva compared to nasopharyngeal swab,[51] which may benefit the detection of viral nucleic acid. The saliva sample has a more complex composition that could affect the sensor performance. Therefore, it is worth evaluating the dynamic response of ssDNA/$Ti_3C_2T_x$ sensors to SARS-CoV-2 N gene in saliva. The real-time sensing results presented in Figure 5d,e indicate that ssDNA/$Ti_3C_2T_x$ sensors maintain a good sensitivity, even when tested in saliva, down to a concentration of 10^5 copies/mL. This study provides the feasibility of detecting SARS-CoV-2 genes using 2D MXene functionalized with ssDNA recognition probes as a promising pathway for rapid detection of SARS-CoV-2 gene. To further investigate the theoretical limit of detection (LOD) of ssDNA/$Ti_3C_2T_x$ sensors, the LODs for SARS-CoV-2 N genes in both buffer and saliva were calculated with a signal-to-noise ratio (SNR) of 3.[52] The relationship between the sensor response and the concentrations in buffer and saliva with a linear fitting model is shown in Figure S3, Supporting Information. The ssDNA/$Ti_3C_2T_x$ sensors exhibit a similar slope and response, with a LOD of $\sim 10^3$ copies/mL in both buffer and saliva, indicating that this platform has a superior sensitivity toward SARS-CoV-2 N genes. These estimations prove themselves to be accurate as they not only sufficiently model the

https://doi.org/10.1021/acsanm.1c03520
ACS Appl. Nano Mater. 2022, 5, 1902−1910

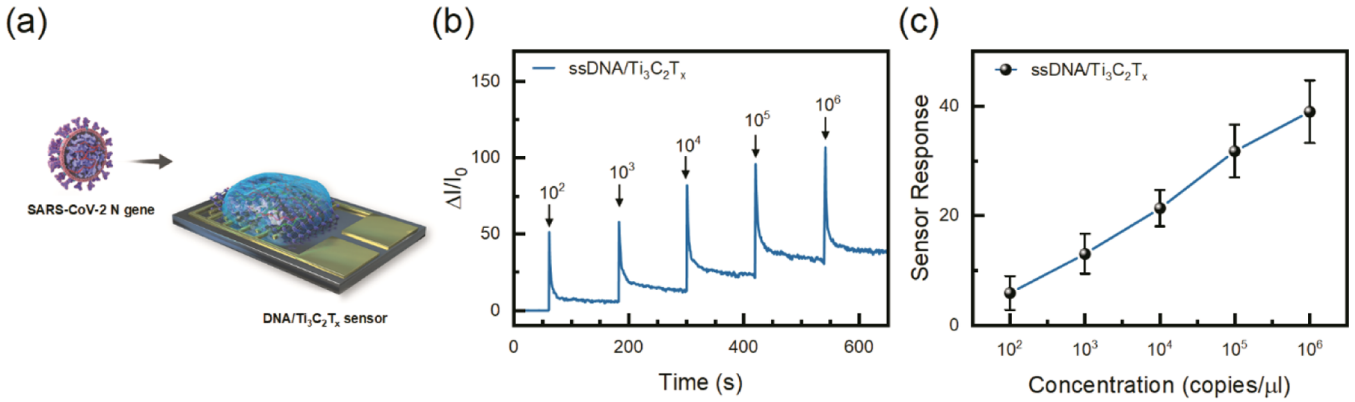

Figure 6. Detection of SARS-CoV-2 N gene from heat-inactivated SARS-CoV-2. (a) Schematic illustration of ssDNA/$Ti_3C_2T_x$ biosensors for SARS-CoV-2 N gene detection. (b) Real-time response of N gene and (c) corresponding response versus concentration plot for ssDNA/$Ti_3C_2T_x$ sensors.

experimental data of both in buffer and saliva but also reflect low variation in these different media.

We also validated the selectivity of ssDNA/$Ti_3C_2T_x$ sensors by preparing and testing oligonucleotide sequences from the closely related N genes of SARS-CoV-2, SARS-CoV-1, and MERS-CoV, all having a concentration of 10^5 copies/mL. As demonstrated in Figure 5f, the ssDNA/$Ti_3C_2T_x$ sensor shows almost no response to SARS-CoV-1 and MERS-CoV N genes, confirming that this biosensing platform possesses sequence-specific recognition for SARS-CoV-2 N gene. The selectivity results also suggest that SARS-CoV-2 N probes are highly specific for SARS-CoV-2 N gene, which is consistent with the agarose gel electrophoresis experiments demonstrating the specificity of SARS-CoV-2 N probes for detecting the N gene of SARS-CoV-2 (Figure S4, Supporting Information).

The detection of clinically relevant targets is essential and important for practical diagnostic development. Thus, the detection of N gene from heat-inactivated SARS-CoV-2 using ssDNA/$Ti_3C_2T_x$ sensors was performed (Figure 6a). As SARS-CoV-2 isolation and propagation require a Biosafety Level 3 (BSL-3) laboratory, the noninfectious SARS-CoV-2 was prepared by heating the virus to 65 °C for 30 min and thus was safe to use under BSL-1 conditions.[53] The N gene target was confirmed by one-step qRT-PCR and agarose gel electrophoresis from heat-inactivated SARS-CoV-2 (Figure S5, Supporting Information). The SARS-CoV-2 N gene sequence contains a single band with a length of 72 base pair (bp), consistent with previous PCR results.[53] The real-time sensing of the ssDNA/$Ti_3C_2T_x$ sensor under various concentrations of N gene from heat-inactivated SARS-CoV-2 is shown in Figure 6b. The sensor exhibits an evident current response increase with increasing the concentration of target gene. Figure 6c shows the relationship between the response values and target concentrations. The ssDNA/$Ti_3C_2T_x$ sensor is ultrasensitive to the SARS-CoV-2 N gene with (i) a low detection limit of less than 10^5 copies/mL and (ii) a nearly linear response over a wide range of concentrations from 10^5 to 10^9 copies/mL, which is suitable for detecting viral loads from the majority of reported patients at the onset of symptoms.[54−56] The sensor response shows slightly lower sensitivity compared to the sensor response in buffer and saliva, caused by a minimized device-to-device variation. The detectable viral load strongly depends on the days after symptom onset, and it has been reported that SARS-CoV-2 could be most reliably detected around symptom onset or a few days thereafter.[57,58] The low detection limit and linear response toward SARS-CoV-2 N gene suggest that MXene-based biosensors fabricated here have the ability to detect low viral load.

Compared with other 2D materials (e.g., graphene and MoS_2), $Ti_3C_2T_x$ core materials present the advantages of unusually high electrical conductivity, functionalized, and hydrophilic surface, providing not only a high signal-to-noise ratio for chemiresistive biosensors but also the ability to precisely tailor their properties for biomolecule sensing through surface modification. Because of the low or even the zero-band-gap electronic structure of graphene, graphene-based biosensors typically show small changes in electrical conductance, limiting their response and sensitivity.[7,11,27] On the other hand, transition-metal dichalcogenides are larger band gap materials and exhibit a higher response but suffer from the intrinsically high noise level.[12,28] Owing to a highly conductive Ti_3C_2 core with abundant hydrophilic surface functionalities, MXene-based materials are an attractive candidate for the development of high-performance biosensing devices.

In conjunction with the recent studies of SARS-CoV-2 detection technologies (Table S2, Supporting Information), the ssDNA/$Ti_3C_2T_x$ biosensing platform reported herein is rather straightforward to use. The use of self-collected saliva samples is less invasive, can also minimize health care worker exposure, and decrease the need for sample collection devices, such as swabs. The nucleic acid electrochemical biosensing proposed here is effective and reliable, which can reduce false positive or negative results. Targeting the N gene ensures the specific detection of SARS-CoV-2 owing to its low rate of mutation compared to the multiple mutations of S genes observed in the three new SARS-CoV-2 variants when COVID-19 pandemic progress. Furthermore, the biosensing technology examined here, which did not use fluorescent probes and laboratory-scale instruments, provides an insight for the preparation of SARS-CoV-2 biosensors with potential for low-cost manufacturing and mass production.

CONCLUSIONS

A DNA primer-functionalized $Ti_3C_2T_x$ biosensor was successfully developed for a highly sensitive, selective, and rapid detection of the N gene of SARS-CoV-2. The sensor response increases with the concentration of the added target DNA. A clear differentiable response to the N gene of SARS-CoV-2 with ssDNA/$Ti_3C_2T_x$ sensors can be observed at a

https://doi.org/10.1021/acsanm.1c03520
ACS Appl. Nano Mater. 2022, 5, 1902−1910

concentration as low as 10^5 copies/mL in artificial saliva, which matches the current detection limits of conventional qPCR testing. The ssDNA/$Ti_3C_2T_x$ biosensor also demonstrates the same performance toward detecting the SARS-CoV-2 N gene in saliva samples. The cross-reactivity of the sensor was confirmed against SARS-CoV-1 and MERS-CoV. The detection mechanism of N gene from SARS-CoV-2 for DNA-functionalized $Ti_3C_2T_x$ is proposed as being dominated by the hybridization of highly selective DNA probes on $Ti_3C_2T_x$ surfaces with SARS-CoV-2 N gene. Under the current COVID-19 outbreak, this study shows the feasibility of developing a real time and highly reliable diagnosis devices for clinical tests based on DNA-functionalized $Ti_3C_2T_x$ MXenes.

EXPERIMENTAL SECTION

Materials. Ti_3AlC_2 (2 g, particle size <40 μm) was purchased from Carbon-Ukraine. Conductive gold ink (UTDAu25) was purchased from UT Dots (Champaign, IL). The plasmid controls of the viruses contain a complete nucleocapsid gene from 2019-nCoV, SARS, and MERS viruses, which were synthesized from Integrated DNA Technologies (IDT, Skokie, IL). The selected oligonucleotide probes were approved by the US Centers for Disease Control and Prevention (CDC) and given in Table S3,[59] Supporting Information: nCOV-N Forward Probe, 5′-GACCCCAAAATCAGCGAAAT-3′, nCOV-N Reverse Probe, and 5′- TCTGGTTACTGCCAGTTGAATCTG-3′. The artificial saliva was purchased from Pickering Laboratories (Mountain View, CA). Heat-inactivated SARS-CoV-2 (strain: 2019-nCoV/USA-WA1/2020, ATCC VR-1986HK) was purchased from American Type Culture Collection (ATCC, VA). All other chemical reagents were of analytical reagent grade and used without further purification. Ultrapure water (>18.3 MΩ) was used throughout the experiment.

Preparation of $Ti_3C_2T_x$ MXene. $Ti_3C_2T_x$ MXene were prepared on the basis of the procedure reported by Gogotsi et al.[38,60] Ti_3AlC_2 powder was selectively etched to remove Al layers in a premixed acid solution of 9M HCl (20 mL) and LiF (3.2 g) and stirred at 200 rpm for 24 h at room temperature. The mixture was washed through several centrifugation cycles with ultrapure water until pH value of the supernatant reached approximately 6. The resulting $Ti_3C_2T_x$ sediment was collected and rewashed with ultrapure water by vacuum filtration using the PVDF membrane with 0.22 μm pore size, subsequently dried in vacuum at 80 °C for 24 h. To obtain delaminated $Ti_3C_2T_x$ dispersion, 100 mg of $Ti_3C_2T_x$ multilayer powder was sonicated in 20 mL of ultrapure water with an ultrasonic bath (Branson, CPX2800H) for 1 h. The bath temperature was controlled at 4 °C to prevent restacking of nanosheets caused by the thermal energy released during sonication. The delaminated $Ti_3C_2T_x$ nanoflakes were collected for fabricating SAR-CoV-2 biosensors.

Fabrication of ssDNA/$Ti_3C_2T_x$ Sensors. First, nanogold ink was printed by a commercial inkjet printer (Dimatix DMP-2850, Fujifilm) on a polyimide substrate containing six pairs of gold interdigitated electrodes with a total active electrode area of 8 mm × 8 mm. Then, the $Ti_3C_2T_x$ solution (5 mg/mL) was sprayed onto interdigitated electrodes using an airbrush (G-233, Master Airbrush) for 10 s. The spray conditions were achieved with an operating pressure of 80 psi, a 0.5 mm of nozzle size, an operating distance of 30 cm between the spray nozzle and substrate, and a steady moving speed of 10 cm/s in all directions. The stock solution of probe DNA solution (10 μM) was thawed on ice and desired concentration of the DNA ligand was prepared. The $Ti_3C_2T_x$ films were then functionalized by casting a 20 μL drop of mixed probe DNA solution (5 μM) and immediately dried under vacuum. The resistance values of the sensor were recorded (Table S4, Supporting Information). No significant changes for 1 μM of DNA loading are due to the insufficient DNA loading on the sensor surface. Both 5 and 10 μM of DNA loadings have similar resistance value, suggesting that 5 μM of DNA loading is enough for SARS-CoV-2 detection. All DNA solutions used in this study were quantified on the NanoDrop 2000 spectrophotometer (Thermo Fisher Scientific).

Characterization and Real-Time Sensing of SARS-CoV-2 Viral Sequences. The surface morphology and microstructure of the $Ti_3C_2T_x$ MXene were examined by scanning electron microscopy (SEM; S-4800, Hitachi), transmission electron microscopy (TEM; Talos 200X, FEI), high-angle annular dark-field scanning electron microscopy (HAADF-STEM), and X-ray diffractometry (XRD; X'Pert Pro, Panalytical) operated at 45 kV and 40 mA using Cu Kα radiation. X-ray photoelectron spectroscopy (XPS; PHI 5000 Versaprobe, ULVAC-PHI) was conducted to investigate chemical components and bonding structures. The N gene sequences were detected by 3% agarose gel electrophoresis at 120 V for 60 min. The DNA agarose gel was imaged by the Bio-Rad imaging system. The electrical performance was measured using a source measure unit (Keithley 2400). The sensor response is defined using the following formula: $\Delta I/I_0 = (I-I_0)/I_0$, where I and I_0 represent the real-time current and the initial current of the sensors, respectively.

ASSOCIATED CONTENT

Supporting Information

The Supporting Information is available free of charge at https://pubs.acs.org/doi/10.1021/acsanm.1c03520.

Figure S1, XPS survey spectra for $Ti_3C_2T_x$ and ssDNA/$Ti_3C_2T_x$; Table S1, atomic concentrations of elements; Figure S2, working mechanism of the biosensor; Figure S3, linear relationship between response and concentration in buffer and saliva; Figure S4, agarose gel electrophoresis of SARS-CoV-2 N gene using SARS-CoV-N probes; Figure S5, agarose gel electrophoresis of N gene from heat-inactivated SARS-CoV-2; Table S2, summary of recent studies for SARS-CoV-2 detection; Table S3, selected sequences for SARS-CoV-2 detection; and Table S4, resistance measurements of biosensors after different concentrations of DNA loading (PDF)

AUTHOR INFORMATION

Corresponding Author

Lia A. Stanciu − *School of Materials Engineering, Purdue University, West Lafayette, Indiana 47907, United States; Birck Nanotechnology Center, Purdue University, West Lafayette, Indiana 47907, United States;* orcid.org/0000-0001-6059-0346; Email: lstanciu@purdue.edu

Authors

Winston Yenyu Chen − *School of Materials Engineering, Purdue University, West Lafayette, Indiana 47907, United States; Birck Nanotechnology Center, Purdue University, West Lafayette, Indiana 47907, United States*

Hang Lin − *Department of Medicinal Chemistry and Molecular Pharmacology and Purdue Center for Cancer Research, Purdue University, West Lafayette, Indiana 47907, United States*

Amit Kumar Barui − *School of Materials Engineering, Purdue University, West Lafayette, Indiana 47907, United States; Birck Nanotechnology Center, Purdue University, West Lafayette, Indiana 47907, United States*

Ana Maria Ulloa Gomez − *School of Materials Engineering, Purdue University, West Lafayette, Indiana 47907, United States; Birck Nanotechnology Center, Purdue University, West Lafayette, Indiana 47907, United States*

Michael K. Wendt − *Department of Medicinal Chemistry and Molecular Pharmacology and Purdue Center for Cancer*

https://doi.org/10.1021/acsanm.1c03520
ACS Appl. Nano Mater. 2022, 5, 1902−1910

Research, Purdue University, West Lafayette, Indiana 47907, United States

Complete contact information is available at: https://pubs.acs.org/10.1021/acsanm.1c03520

Author Contributions

[⊥]W.Y.C. and H.L. contributed equally to this work.

Notes

The authors declare no competing financial interest.

■ ACKNOWLEDGMENTS

The authors wish to thank the Birck Nanotechnology Center at Purdue University for providing equipment and technical support. This work was supported by NSF/CBET#2027554 titled RAPID: A Surface-Based Detection Platform for SARS-CoV-2.

■ REFERENCES

(1) Coronavirus disease 2019. *COVID-19 Situation Report*; World Health Organization, 2020.

(2) Corman, V. M.; Landt, O.; Kaiser, M.; Molenkamp, R.; Meijer, A.; Chu, D. K.; Bleicker, T.; Brunink, S.; Schneider, J.; Schmidt, M. L.; Mulders, D. G.; Haagmans, B. L.; van der Veer, B.; van den Brink, S.; Wijsman, L.; Goderski, G.; Romette, J. L.; Ellis, J.; Zambon, M.; Peiris, M.; Goossens, H.; Reusken, C.; Koopmans, M. P.; Drosten, C. Detection of 2019 novel coronavirus (2019-nCoV) by real-time RT-PCR. *Eurosurveillance* **2020**, *25*, No. 2000045.

(3) Muenchhoff, M.; Mairhofer, H.; Nitschko, H.; Grzimek-Koschewa, N.; Hoffmann, D.; Berger, A.; Rabenau, H.; Widera, M.; Ackermann, N.; Konrad, R.; Zange, S.; Graf, A.; Krebs, S.; Blum, H.; Sing, A.; Liebl, B.; Wölfel, R.; Ciesek, S.; Drosten, C.; Protzer, U.; Boehm, S.; Keppler, O. T. Multicentre comparison of quantitative PCR-based assays to detect SARS-CoV-2, Germany, March 2020. *Eurosurveillance* **2020**, *25*, No. 2001057.

(4) Udugama, B.; Kadhiresan, P.; Kozlowski, H. N.; Malekjahani, A.; Osborne, M.; Li, V. Y. C.; Chen, H.; Mubareka, S.; Gubbay, J. B.; Chan, W. C. W. Diagnosing COVID-19: The Disease and Tools for Detection. *ACS Nano* **2020**, *14*, 3822−3835.

(5) Soler, M.; Estevez, M. C.; Cardenosa-Rubio, M.; Astua, A.; Lechuga, L. M. How Nanophotonic Label-Free Biosensors Can Contribute to Rapid and Massive Diagnostics of Respiratory Virus Infections: COVID-19 Case. *ACS Sens.* **2020**, *5*, 2663−2678.

(6) Qiu, G.; Gai, Z.; Tao, Y.; Schmitt, J.; Kullak-Ublick, G. A.; Wang, J. Dual-Functional Plasmonic Photothermal Biosensors for Highly Accurate Severe Acute Respiratory Syndrome Coronavirus 2 Detection. *ACS Nano* **2020**, *14*, 5268−5277.

(7) Seo, G.; Lee, G.; Kim, M. J.; Baek, S. H.; Choi, M.; Ku, K. B.; Lee, C. S.; Jun, S.; Park, D.; Kim, H. G.; Kim, S. J.; Lee, J. O.; Kim, B. T.; Park, E. C.; Kim, S. I. Rapid Detection of COVID-19 Causative Virus (SARS-CoV-2) in Human Nasopharyngeal Swab Specimens Using Field-Effect Transistor-Based Biosensor. *ACS Nano* **2020**, *14*, 5135−5142.

(8) Pinals, R. L.; Ledesma, F.; Yang, D.; Navarro, N.; Jeong, S.; Pak, J. E.; Kuo, L.; Chuang, Y.-C.; Cheng, Y.-W.; Sun, H.-Y.; Landry, M. P. Rapid SARS-CoV-2 Spike Protein Detection by Carbon Nanotube-Based Near-Infrared Nanosensors. *Nano Lett.* **2021**, *21*, 2272−2280.

(9) Yousefi, H.; Mahmud, A.; Chang, D.; Das, J.; Gomis, S.; Chen, J. B.; Wang, H.; Been, T.; Yip, L.; Coomes, E.; Li, Z.; Mubareka, S.; McGeer, A.; Christie, N.; Gray-Owen, S.; Cochrane, A.; Rini, J. M.; Sargent, E. H.; Kelley, S. O. Detection of SARS-CoV-2 Viral Particles Using Direct, Reagent-Free Electrochemical Sensing. *J. Am. Chem. Soc.* **2021**, *143*, 1722−1727.

(10) Vermisoglou, E.; Panáček, D.; Jayaramulu, K.; Pykal, M.; Frébort, I.; Kolář, M.; Hajdúch, M.; Zbořil, R.; Otyepka, M. Human virus detection with graphene-based materials. *Biosens. Bioelectron.* **2020**, *166*, No. 112436.

(11) Loan, P. T.; Zhang, W.; Lin, C. T.; Wei, K. H.; Li, L. J.; Chen, C. H. Graphene/MoS(2) heterostructures for ultrasensitive detection of DNA hybridisation. *Adv. Mater.* **2014**, *26*, 4838−4844.

(12) Liu, J.; Chen, X.; Wang, Q.; Xiao, M.; Zhong, D.; Sun, W.; Zhang, G.; Zhang, Z. Ultrasensitive Monolayer MoS2 Field-Effect Transistor Based DNA Sensors for Screening of Down Syndrome. *Nano Lett.* **2019**, *19*, 1437−1444.

(13) Lu, C.; Liu, Y.; Ying, Y.; Liu, J. Comparison of MoS2, WS2, and Graphene Oxide for DNA Adsorption and Sensing. *Langmuir* **2017**, *33*, 630−637.

(14) Naguib, M.; Kurtoglu, M.; Presser, V.; Lu, J.; Niu, J.; Heon, M.; Hultman, L.; Gogotsi, Y.; Barsoum, M. W. Two-dimensional nanocrystals produced by exfoliation of Ti_3AlC_2. *Adv. Mater.* **2011**, *23*, 4248−4253.

(15) Anasori, B.; Lukatskaya, M. R.; Gogotsi, Y. 2D Metal Carbides and Nitrides (MXenes) for Energy Storage. *Nat. Rev. Mater.* **2017**, *2*, No. 16098.

(16) Lim, K. R. G.; Handoko, A. D.; Nemani, S. K.; Wyatt, B.; Jiang, H. Y.; Tang, J.; Anasori, B.; Seh, Z. W. Rational Design of Two-Dimensional Transition Metal Carbide/Nitride (MXene) Hybrids and Nanocomposites for Catalytic Energy Storage and Conversion. *ACS Nano* **2020**, *14*, 10834−10864.

(17) Pang, J.; Mendes, R. G.; Bachmatiuk, A.; Zhao, L.; Ta, H. Q.; Gemming, T.; Liu, H.; Liu, Z.; Rummeli, M. H. Applications of 2D MXenes in Energy Conversion and Storage Systems. *Chem. Soc. Rev.* **2019**, *48*, 72−133.

(18) Vural, M.; Pena-Francesch, A.; Bars-Pomes, J.; Jung, H.; Gudapati, H.; Hatter, C. B.; Allen, B. D.; Anasori, B.; Ozbolat, I. T.; Gogotsi, Y.; Demirel, M. C. Inkjet Printing of Self-Assembled 2D Titanium Carbide and Protein Electrodes for Stimuli-Responsive Electromagnetic Shielding. *Adv. Funct. Mater.* **2018**, *28*, No. 1801972.

(19) Rasool, K.; Pandey, R. P.; Rasheed, P. A.; Buczek, S.; Gogotsi, Y.; Mahmoud, K. A. Water Treatment and Environmental Remediation Applications of Two-Dimensional Metal Carbides (MXenes). *Mater. Today* **2019**, *30*, 80−102.

(20) Peng, J.; Chen, X.; Ong, W. J.; Zhao, X.; Li, N. Surface and Heterointerface Engineering of 2D MXenes and Their Nanocomposites: Insights into Electro- and Photocatalysis. *Chem* **2019**, *5*, 18−50.

(21) Gogotsi, Y.; Anasori, B. The Rise of MXenes. *ACS Nano* **2019**, *13*, 8491−8494.

(22) Zhang, Q.; Wang, F.; Zhang, H.; Zhang, Y.; Liu, M.; Liu, Y. Universal Ti3C2 MXenes Based Self-Standard Ratiometric Fluorescence Resonance Energy Transfer Platform for Highly Sensitive Detection of Exosomes. *Anal. Chem.* **2018**, *90*, 12737−12744.

(23) Sheng, A.; Wang, P.; Yang, J.; Tang, L.; Chen, F.; Zhang, J. MXene Coupled with CRISPR-Cas12a for Analysis of Endotoxin and Bacteria. *Anal. Chem.* **2021**, *93*, 4676−4681.

(24) Lin, H.; Chen, Y.; Shi, J. Insights into 2D MXenes for versatile biomedical applications: current advances and challenges ahead. *Adv. Sci.* **2018**, *5*, No. 1800518.

(25) Szuplewska, A.; Kulpinska, D.; Dybko, A.; Chudy, M.; Jastrzebska, A. M.; Olszyna, A.; Brzozka, Z. Future Applications of MXenes in Biotechnology, Nanomedicine, and Sensors. *Trends Biotechnol.* **2020**, *38*, 264−279.

(26) Yadav, P.; Cao, Z.; Barati Farimani, A. DNA Detection with Single-Layer Ti3C2 MXene Nanopore. *ACS Nano* **2021**, *15*, 4861−4869.

(27) Xu, S.; Zhan, J.; Man, B.; Jiang, S.; Yue, W.; Gao, S.; Guo, C.; Liu, H.; Li, Z.; Wang, J.; Zhou, Y. Real-time reliable determination of binding kinetics of DNA hybridization using a multi-channel graphene biosensor. *Nat. Commun.* **2017**, *8*, No. 14902.

(28) Kim, S. J.; Koh, H. J.; Ren, C. E.; Kwon, O.; Maleski, K.; Cho, S. Y.; Anasori, B.; Kim, C. K.; Choi, Y. K.; Kim, J.; Gogotsi, Y.; Jung, H. T. Metallic $Ti_3C_2T_x$ MXene Gas Sensors with Ultrahigh Signal-to-Noise Ratio. *ACS Nano* **2018**, *12*, 986−993.

(29) He, S.; Song, B.; Li, D.; Zhu, C.; Qi, W.; Wen, Y.; Wang, L.; Song, S.; Fang, H.; Fan, C. A Graphene Nanoprobe for Rapid,

Sensitive, and Multicolor Fluorescent DNA Analysis. *Adv. Funct. Mater.* **2010**, *20*, 453−459.
(30) Manzanares-Palenzuela, C. L.; Pourrahimi, A. M.; Gonzalez-Julian, J.; Sofer, Z.; Pykal, M.; Otyepka, M.; Pumera, M. Interaction of single- and double-stranded DNA with multilayer MXene by fluorescence spectroscopy and molecular dynamics simulations. *Chem. Sci.* **2019**, *10*, 10010−10017.
(31) Huang, J.; Li, Z.; Mao, Y.; Li, Z. Progress and biomedical applications of MXenes. *Nano Select* **2021**, *2*, 1480−1508.
(32) Chen, Z.; Zhang, Z.; Zhai, X.; Li, Y.; Lin, L.; Zhao, H.; Bian, L.; Li, P.; Yu, L.; Wu, Y.; Lin, G. Rapid and Sensitive Detection of anti-SARS-CoV-2 IgG, Using Lanthanide-Doped Nanoparticles-Based Lateral Flow Immunoassay. *Anal. Chem.* **2020**, *92*, 7226−7231.
(33) Wang, H.; Li, H.; Huang, Y.; Xiong, M.; Wang, F.; Li, C. A label-free electrochemical biosensor for highly sensitive detection of gliotoxin based on DNA nanostructure/MXene nanocomplexes. *Biosens. Bioelectron.* **2019**, *142*, No. 111531.
(34) Okubo, M.; Sugahara, A.; Kajiyama, S.; Yamada, A. MXene as a Charge Storage Host. *Acc. Chem. Res.* **2018**, *51*, 591−599.
(35) Ding, L.; Wei, Y.; Li, L.; Zhang, T.; Wang, H.; Xue, J.; Ding, L. X.; Wang, S.; Caro, J.; Gogotsi, Y. MXene Molecular Sieving Membranes for Highly Efficient Gas Separation. *Nat. Commun.* **2018**, *9*, No. 155.
(36) Xu, J.; Peng, T.; Qin, X.; Zhang, Q.; Liu, T.; Dai, W.; Chen, B.; Yu, H.; Shi, S. Recent advances in 2D MXenes: preparation, intercalation and applications in flexible devices. *J. Mater. Chem. A* **2021**, *9*, 14147−14171.
(37) Chen, C.; Boota, M.; Urbankowski, P.; Anasori, B.; Miao, L.; Jiang, J.; Gogotsi, Y. Effect of Glycine Functionalization of 2D Titanium Carbide (MXene) on Charge Storage. *J. Mater. Chem. A* **2018**, *6*, 4617−4622.
(38) Alhabeb, M.; Maleski, K.; Anasori, B.; Lelyukh, P.; Clark, L.; Sin, S.; Gogotsi, Y. Guidelines for Synthesis and Processing of Two-Dimensional Titanium Carbide ($Ti_3C_2T_x$ MXene). *Chem. Mater.* **2017**, *29*, 7633−7644.
(39) Peng, C.; Yang, X.; Li, Y.; Yu, H.; Wang, H.; Peng, F. Hybrids of Two-Dimensional Ti_3C_2 and TiO_2 Exposing {001} Facets toward Enhanced Photocatalytic Activity. *ACS Appl. Mater. Interfaces* **2016**, *8*, 6051−6060.
(40) Halim, J.; Lukatskaya, M. R.; Cook, K. M.; Lu, J.; Smith, C. R.; Naslund, L. A.; May, S. J.; Hultman, L.; Gogotsi, Y.; Eklund, P.; Barsoum, M. W. Transparent Conductive Two-Dimensional Titanium Carbide Epitaxial Thin Films. *Chem. Mater.* **2014**, *26*, 2374−2381.
(41) Shah, S. A.; Habib, T.; Gao, H.; Gao, P.; Sun, W.; Green, M. J.; Radovic, M. Template-Free 3D Titanium Carbide ($Ti_3C_2T_x$) MXene Particles Crumpled by Capillary Forces. *Chem. Commun.* **2017**, *53*, 400−403.
(42) Herne, T. M.; Tarlov, M. J. Characterization of DNA Probes Immobilized on Gold Surfaces. *J. Am. Chem. Soc.* **1997**, *119*, 8916−8920.
(43) Lu, R.; Zhao, X.; Li, J.; Niu, P.; Yang, B.; Wu, H.; Wang, W.; Song, H.; Huang, B.; Zhu, N.; Bi, Y.; Ma, X.; Zhan, F.; Wang, L.; Hu, T.; Zhou, H.; Hu, Z.; Zhou, W.; Zhao, L.; Chen, J.; Meng, Y.; Wang, J.; Lin, Y.; Yuan, J.; Xie, Z.; Ma, J.; Liu, W. J.; Wang, D.; Xu, W.; Holmes, E. C.; Gao, G. F.; Wu, G.; Chen, W.; Shi, W.; Tan, W. Genomic characterisation and epidemiology of 2019 novel coronavirus: implications for virus origins and receptor binding. *The Lancet* **2020**, *395*, 565−574.
(44) Shang, J.; Wan, Y.; Luo, C.; Ye, G.; Geng, Q.; Auerbach, A.; Li, F. Cell entry mechanisms of SARS-CoV-2. *Proc. Natl. Acad. Sci. U.S.A.* **2020**, *117*, 11727−11734.
(45) Walls, A. C.; Park, Y. J.; Tortorici, M. A.; Wall, A.; McGuire, A. T.; Veesler, D. Structure, Function, and Antigenicity of the SARS-CoV-2 Spike Glycoprotein. *Cell* **2020**, *181*, 281−292.e6.
(46) Korber, B.; Fischer, W. M.; Gnanakaran, S.; Yoon, H.; Theiler, J.; Abfalterer, W.; Hengartner, N.; Giorgi, E. E.; Bhattacharya, T.; Foley, B.; Hastie, K. M.; Parker, M. D.; Partridge, D. G.; Evans, C. M.; Freeman, T. M.; de Silva, T. I.; Sheffield, C.-G. G.; McDanal, C.; Perez, L. G.; Tang, H.; Moon-Walker, A.; Whelan, S. P.; LaBranche, C. C.; Saphire, E. O.; Montefiori, D. C.; et al. Tracking Changes in SARS-CoV-2 Spike: Evidence that D614G Increases Infectivity of the COVID-19 Virus. *Cell* **2020**, *182*, 812−827.e19.
(47) Dutta, N. K.; Mazumdar, K.; Gordy, J. T. The Nucleocapsid Protein of SARS-CoV-2: a Target for Vaccine Development. *J. Virol.* **2020**, *94*, No. e00647-20.
(48) Holmes, K. V.; Enjuanes, L. Virology. The SARS coronavirus: a postgenomic era. *Science* **2003**, *300*, 1377−1378.
(49) Cong, Y.; Ulasli, M.; Schepers, H.; Mauthe, M.; V'Kovski, P.; Kriegenburg, F.; Thiel, V.; de Haan, C. A. M.; Reggiori, F. Nucleocapsid Protein Recruitment to Replication-Transcription Complexes Plays a Crucial Role in Coronaviral Life Cycle. *J. Virol.* **2020**, *94*, No. e01925-19.
(50) Arnaout, R.; Lee, R. A.; Lee, G. R.; Callahan, C.; Cheng, A.; Yen, C. F.; Smith, K. P.; Arora, R.; Kirby, J. E. The Limit of Detection Matters: The Case for Benchmarking Severe Acute Respiratory Syndrome Coronavirus 2 Testing. *Clin. Infect. Dis.* **2021**, e3042−e3046.
(51) Butler-Laporte, G.; Lawandi, A.; Schiller, I.; Yao, M.; Dendukuri, N.; McDonald, E. G.; Lee, T. C. Comparison of Saliva and Nasopharyngeal Swab Nucleic Acid Amplification Testing for Detection of SARS-CoV-2: A Systematic Review and Meta-analysis. *JAMA Intern. Med.* **2021**, *181*, 353−360.
(52) Lee, E.; VahidMohammadi, A.; Yoon, Y. S.; Beidaghi, M.; Kim, D. J. Two-Dimensional Vanadium Carbide MXene for Gas Sensors with Ultrahigh Sensitivity toward Nonpolar Gases. *ACS Sens.* **2019**, *4*, 1603−1611.
(53) Smyrlaki, I.; Ekman, M.; Lentini, A.; Rufino de Sousa, N.; Papanicolaou, N.; Vondracek, M.; Aarum, J.; Safari, H.; Muradrasoli, S.; Rothfuchs, A. G.; Albert, J.; Hogberg, B.; Reinius, B. Massive and rapid COVID-19 testing is feasible by extraction-free SARS-CoV-2 RT-PCR. *Nat. Commun.* **2020**, *11*, No. 4812.
(54) Bhalla, N.; Pan, Y.; Yang, Z.; Payam, A. F. Opportunities and Challenges for Biosensors and Nanoscale Analytical Tools for Pandemics: COVID-19. *ACS Nano* **2020**, *14*, 7783−7807.
(55) Rodriguez, N. M.; Linnes, J. C.; Fan, A.; Ellenson, C. K.; Pollock, N. R.; Klapperich, C. M. Paper-Based RNA Extraction, in Situ Isothermal Amplification, and Lateral Flow Detection for Low-Cost, Rapid Diagnosis of Influenza A (H1N1) from Clinical Specimens. *Anal. Chem.* **2015**, *87*, 7872−7879.
(56) Oh, M. D.; Park, W. B.; Choe, P. G.; Choi, S. J.; Kim, J. I.; Chae, J.; Park, S. S.; Kim, E. C.; Oh, H. S.; Kim, E. J.; Nam, E. Y.; Na, S. H.; Kim, D. K.; Lee, S. M.; Song, K. H.; Bang, J. H.; Kim, E. S.; Kim, H. B.; Park, S. W.; Kim, N. J. Viral Load Kinetics of MERS Coronavirus Infection. *N. Engl. J. Med.* **2016**, *375*, 1303−1305.
(57) Zou, L.; Ruan, F.; Huang, M.; Liang, L.; Huang, H.; Hong, Z.; Yu, J.; Kang, M.; Song, Y.; Xia, J.; Guo, Q.; Song, T.; He, J.; Yen, H.-L.; Peiris, M.; Wu, J. SARS-CoV-2 Viral Load in Upper Respiratory Specimens of Infected Patients. *N. Engl. J. Med.* **2020**, *382*, 1177−1179.
(58) Walsh, K. A.; Jordan, K.; Clyne, B.; Rohde, D.; Drummond, L.; Byrne, P.; Ahern, S.; Carty, P. G.; O'Brien, K. K.; O'Murchu, E.; O'Neill, M.; Smith, S. M.; Ryan, M.; Harrington, P. SARS-CoV-2 detection, viral load and infectivity over the course of an infection. *J. Infect.* **2020**, *81*, 357−371.
(59) Prevention, U. C. f.D. C. A., 2019-Novel Coronavirus (2019-nCoV) Real-time rRT-PCR Primers and Probes, 2020.
(60) Chen, W. Y.; Lai, S. N.; Yen, C. C.; Jiang, X.; Peroulis, D.; Stanciu, L. A. Surface Functionalization of $Ti_3C_2T_x$ MXene with Highly Reliable Superhydrophobic Protection for Volatile Organic Compounds Sensing. *ACS Nano* **2020**, *14*, 11490−11501.

https://doi.org/10.1021/acsanm.1c03520
ACS Appl. Nano Mater. 2022, 5, 1902−1910